1 **Stem hydraulic capacitance decreases with drought stress: implications for modelling tree**

2 **hydraulics in the Mediterranean oak *Quercus ilex***

3 Running title: Seasonality in stem hydraulic capacitance

4 Salomón, Roberto L[1,2]; Limousin, Jean Marc[3]; Ourcival, Jean Marc[3]; Rodríguez-Calcerrada, Jesús[1];

5 Steppe, Kathy[2]

6 [1] Forest Genetics and Ecophysiology Research Group, E.T.S. Forestry Engineering, Technical

7 University of Madrid, Ciudad Universitaria s/n, 28040, Madrid, Spain

8 [2] Laboratory of Plant Ecology, Department of Applied Ecology and Environmental Biology, Faculty of

9 Bioscience Engineering, Ghent University, Coupure links 653, B-9000 Ghent, Belgium

10 [3] Centre d'Ecologie Fonctionnelle et Evolutive CEFE, CNRS, UMR 5175, 1919 route de Mende, F-34293

11 Montpellier, Cedex 5, France

12 Corresponding author: Salomón, Roberto L.; email address:

13 RobertoLuis.SalomonMoreno@UGent.be

14 **Abstract**

15 Hydraulic modelling is a primary tool to predict plant performance in future drier scenarios.

16 However, as most tree models are validated under non-stress conditions they may fail when water

17 becomes limiting. To simulate tree hydraulic functioning under moist and dry conditions, the current

18 version of a water flow and storage mechanistic model was further developed by implementing

19 equations that describe variation in xylem hydraulic resistance ($R_X$) and stem hydraulic capacitance

20 ($C_S$) with predawn water potential ($\Psi_{PD}$). The model was applied in a Mediterranean forest

21 experiencing intense summer drought, where six *Quercus ilex* trees were instrumented to monitor

22 stem diameter variations and sap flow, concurrently with measurements of predawn and midday leaf

23 water potential. Best model performance was observed when $C_S$ was allowed to decrease with

24 decreasing $\Psi_{PD}$. Hydraulic capacitance decreased from 62 to 25 kg m$^{-3}$ MPa$^{-1}$ across the growing

25 season. In parallel, tree transpiration decreased to a greater extent than the capacitive water release

26 and the contribution of stored water to transpiration increased from 2.0% to 5.1%. Our results

27 demonstrate the importance of stored water and seasonality in $C_S$ for tree hydraulic functioning, and

28 they suggest that $C_S$ should be considered to predict the drought-response of trees with models.

29 **Keywords:** radial stem growth, drought, hydraulic conductance, process-based modelling, holm oak,

30 stem water storage, hydraulic function

31

**1 Introduction**

As soil dries and atmospheric vapor pressure deficit intensifies, xylem conduits are subjected to lower water potential and may eventually cavitate, thus limiting tree water transport. Xylem vulnerability to drought-induced cavitation has been measured in hundreds of species as the main attribute to quantify tree resistance to drought (Choat *et al.*, 2012; Sperry & Love, 2015). A growing body of evidence points, however, to a complementary factor involved in drought resistance: the radial water flow in stems to maintain tree hydraulic integrity by buffering changes in xylem water potential and limiting cavitation of xylem conduits (Goldstein *et al.*, 1998; Meinzer *et al.*, 2003; Steppe & Lemeur, 2004; Scholz *et al.*, 2007; Steppe *et al.*, 2012; McCulloh *et al.*, 2014). In this way, plant tolerance to drought does not solely rely on inherent xylem resistance to cavitation, but also on the radial capacitive release of stored water from elastic-living tissues that transiently reduces xylem tension at a given rate of flow and hence cavitation. Accordingly, a trade-off between hydraulic capacitance and structural traits involved in xylem resistance to cavitation has been observed across a wide range of woody species (Meinzer *et al.*, 2008, 2009). Nevertheless, the role of hydraulic capacitance in plant hydraulics has been traditionally overshadowed by the study of drought-induced cavitation and the vulnerability of xylem to changes in water potential (Meinzer *et al.*, 2009; McCulloh *et al.*, 2014; Epila *et al.*, 2017).

Hydraulic modelling is a key tool to mechanistically understand how trees cope with severe and intense drought events (Mencuccini *et al.*, 2015; Steppe *et al.*, 2015a). Mechanistic models developed for well-watered conditions commonly use static parameters to describe constant xylem hydraulic conductance (Steppe *et al.*, 2006, 2008a; Verbeeck *et al.*, 2007; Zweifel *et al.*, 2007; De Schepper & Steppe, 2010), whereas variable hydraulic conductance as a function of water potential has been successfully implemented as the soil dries out (Sperry *et al.*, 1998; Baert *et al.*, 2015; Mencuccini *et al.*, 2015). Likewise, static parameters are used to describe hydraulic capacitance (e.g. Sperry *et al.*, 1998; Steppe *et al.*, 2006; Zweifel *et al.*, 2007; Baert *et al.*, 2015); however, none of these models consider the variability in stem hydraulic capacitance, although stem water reservoirs

58  are progressively depleted under dry conditions (Scholz *et al.*, 2007, 2008; Verbeeck *et al.*, 2007;

59  Betsch *et al.*, 2011; Kocher *et al.*, 2013; Matheny *et al.*, 2015). Accounting for the dynamic drought

60  response of both hydraulic conductance and capacitance could improve model performance under a

61  wide range of environmental conditions and extended time frames (Steppe *et al.*, 2008b). Model

62  refinement via integration of tree drought responses has therefore been encouraged to advance in

63  our mechanistic understanding of tree hydraulic functioning in future drier scenarios (Verbeeck *et al.*,

64  2007; Baert *et al.*, 2015; Mencuccini *et al.*, 2015; Steppe *et al.*, 2015a, 2015b).

65  In this study, we aimed at modelling tree hydraulic functioning in field-grown *Quercus ilex* L. under

66  wet to dry conditions by taking into account the dynamic nature of both xylem resistance to water

67  transport ($R_X$) and stem hydraulic capacitance ($C_S$). For this purpose, process-level equations that

68  describe the relationship of $R_X$ and $C_S$ with predawn water potential ($\Psi_{PD}$) have been implemented in

69  the current version of a sophisticated mechanistic model that integrates tree water transport

70  dynamics and stem diameter variations (Steppe *et al.*, 2006, 2008a; De Swaef *et al.*, 2015). Water

71  reservoirs are defined here as the elastic tissues subjected to reversible diel cycles of water release

72  and refill to avoid xylem cavitation. Inelastic water release from cavitated xylem conduits under

73  negative water potential (Tyree & Ewers, 1991; Hölttä *et al.*, 2009) is neglected because the rapid

74  reversibility of this phenomenon remains a matter of debate (Brodersen & McElrone, 2013; Cochard

75  & Delzon, 2013). An advantage of this approach is that measurements are not destructive, since the

76  model is driven by sap flow and $\Psi_{PD}$, and calibrated against stem diameter variations and xylem

77  water potential at midday. As these variables can be monitored with peripheral devices and by

78  sampling a small number of leaves, the hydraulic functioning of surveyed trees can be continuously

79  modelled and research is not restricted to discrete observations.

80  We hypothesize that including daily variations in $R_X$ and $C_S$ as a function of $\Psi_{PD}$ improves model

81  accuracy in predicting stem diameter variations and xylem water potential during the dry season.

82  Contrarily, we predict that variability in $R_X$ and $C_S$ may not improve model performance during the

83  wet season as $R_X$ and $C_S$ are expected to remain constant. The integrated root−to−leaf $R_X$ was

4

84      modelled as function of $\Psi_{PD}$ using a negative exponential curve (Baert *et al.*, 2015), an alternative

85      approach to estimate the integrated root–to–leaf hydraulic conductance ($K_X = 1/ R_X$) and generate

86      vulnerability curves. Furthermore, a new equation defining the relationship between $C_S$ and $\Psi_{PD}$ was

87      developed using the shape of water desorption curves and cumulative water release curves reported

88      for several species (Zweifel *et al.*, 2000; Meinzer *et al.*, 2003, 2009; Steppe *et al.*, 2006; Barnard *et al.*,

89      2011; McCulloh *et al.*, 2014). Both magnitude of the decrease in $C_S$ during the dry season and

90      contribution of stored water to the transpiration stream were evaluated. Simulated cumulative water

91      release from internal storage pools was compared with estimates of stem water refilling at the end

92      of the dry season after first autumn heavy rains. Likewise, the simulated vulnerability curve was

93      compared to the vulnerability curves obtained by measurements at the organ scale in the same

94      experimental site (Limousin *et al.*, 2010a; Martin-StPaul *et al.*, 2014).

95      **2 Materials and methods**

96      **2.1 Site description**

97      The study site is located in the Puéchabon State Forest (Montpellier, France) in a stand dominated by

98      *Q. ilex* (43$^o$44'29'' N, 3$^o$35'45'' E, 270 m.a.s.l.). The stand has been historically subjected to periodic

99      coppicing, with the last cut being performed in 1942. Nowadays, top canopy height is 5.5 m, stand

100    density is 4700 stems ha$^{-1}$, and most stems (> 70%) range in diameter at breast height (DBH) from 4

101    to 10 cm. *Buxus sempervirens* L., *Phyllirea latifolia* L., *Pistacia terebinthus* L. and *Juniperus oxycedrus*

102    L. are the main species of the understory layer. The area has a Mediterranean-type climate: annual

103    mean temperature is 13.4 $^o$C, annual precipitation is 907 mm, and 80% of this amount falls during

104    winter and autumn, when temperatures are lower (Limousin *et al.*, 2009).  A weather station located

105    at the experimental site was used to monitor meteorological conditions. Air temperature, relative

106    humidity (MP100, Rotronic, Bassersdorf, Switzerland), and rainfall (tipping bucket rain gauge

107    ARG100, Environmental Measurements Ltd, Sunderland, UK) were measured every minute and

108   averaged every 30 minutes with a data logger (model 21X, Campbell Scientific Ltd, Shepshed, UK).

109   More details on the experimental site are available in Rambal *et al.* (2014).

110   **2.2 Tree and soil measurements**

111   Six *Q. ilex* trees (see Table 1) were instrumented to continuously monitor sap flow and stem diameter

112   variations. We selected data from the year 2009 because it  was characterized by a strong and typical

113   summer drought between mid-July and mid-September, and due to data availability on leaf water

114   potential at predawn and midday in the instrumented trees during the summer.

115   Sap flux density (g cm$^{-2}$ h$^{-1}$) was continuously monitored with thermal dissipation probes (Granier,

116   1985). Probe pairs were inserted at 1.2 m height with a vertical separation of 10 cm. Probes were

117   oriented facing north to avoid direct solar heating, and were protected from rain and radiation by

118   aluminum cover. Temperature difference between the probes was registered every 5 minutes, and

119   averaged and recorded every 30 minutes with a data logger (model CR10X, Campbell Scientific). Sap

120   flux density was calculated considering zero flow from the absolute maximum temperature

121   difference over 2-day running periods. Sap flux density was upscaled to the tree level to obtain sap

122   flow ($F_{STEM}$, g h$^{-1}$) by multiplying sap flux density by sapwood area. Sapwood area was estimated from

123   an allometric relationship between tree DBH and sapwood area obtained from 18 additional trees

124   (Limousin *et al.*, 2009). For further details about $F_{STEM}$ measurements see Limousin et al. (2009).

125   Stem circumference variations were recorded using automatic band dendrometers (ELPA-98,

126   University of Oulu, Oulu, Finland). Dendrometers were just below the thermal dissipation probes,

127   and the outer layer of dead bark was removed prior to installation. Circumference variations were

128   registered every 5 minutes and recorded every 30 minutes with a data logger (model CR1000;

129   Campbell Scientific Ltd, Shepshed, UK) and transformed to stem diameter variations (ΔD, μm). For

130   further details about ΔD measurements see Lempereur et al. (2015).

131   Leaf water potential ($\Psi_{LEAF}$, MPa) was measured with a pressure chamber (PMS1000, PMS

132   Instruments, Corvallis, OR, USA) on DOYs 114, 176, 208, 234 and 310 during the 2009 growing season

6

133 (23 April, 24 June, 26 July, 21 August, 5 November, respectively) at predawn (before 06:00 h) and

134 midday (14:00 h). Two leaves were sampled per tree and a third leaf was sampled if the observed

135 difference between measurements was higher than 0.2 MPa. Samples were taken at similar tree

136 heights and measurements were performed within 1 min after leaf excision. Leaf water potential was

137 measured in four of the six trees instrumented for $F_{STEM}$ and $\Delta D$ measurements. Average $\Psi_{LEAF}$ of

138 these four trees was used for the two remaining trees.

139 The discrete measurements of $\Psi_{PD}$ were interpolated on a daily basis using modelled soil water

140 storage (SWS, mm). Daily soil water storage was modelled using the soil water balance module of the

141 SIERRA vegetation model driven by daily values of solar radiation, minimum and maximum

142 temperature and precipitation (Mouillot *et al.*, 2001; Ruffault *et al.*, 2013). Soil water storage and $\Psi_{PD}$

143 were related by a Campbell-type retention curve (Campbell, 1974). The soil water storage model was

144 validated against measurements of SWS integrated over a rooting depth of 4.5 m and performed at

145 approximately monthly intervals from 1998 to 2009 using a neutron moisture gauge (see Rambal *et*

146 *al.* 2003 for further details). The relationship between modelled and measured SWS displayed a good

147 agreement ($R^2$ = 0.92; p < 0.0001; RMSE = 16 mm; n = 90), as well as the relationship between

148 modelled and measured $\Psi_{PD}$ ($R^2$ = 0.73; p < 0.0001; RMSE = 0.71 MPa; n = 95). Despite the good fit

149 obtained between SWS and $\Psi_{PD}$ on an annual basis, $\Psi_{PD}$ was underestimated by the soil water

150 balance model during summer drought. To correct daily simulated values of $\Psi_{PD}$ in summer,

151 optimized parameters for each tree were selected to account for spatial heterogeneity in leaf area

152 index, soil texture and stone fraction.

153 **2.3 Mechanistic tree modelling**

154 **2.3.1 Model description**

155 The current version of a mechanistic water flow and storage model (Steppe *et al.*, 2008a) was used to

156 study the hydraulic functioning of *Q. ilex* trees. Briefly, the model is composed of two interconnected

157 sub-models describing dynamics in tree water transport and stem diameter variations, in which $F_{STEM}$

158    dynamics are intimately linked to stem ΔD by radial water flow between the xylem and the outer

159    tissues. Note that "stem" refers to the tree trunk, so that branches are excluded for model simplicity.

160    The model assumes the xylem as a rigid cylinder (xylem compartment) surrounded by an elastic outer

161    ring composed of cells of cambium, phloem and bark (storage compartment) responsible for diel

162    shrinkage and swelling (Steppe *et al.*, 2006). Therefore, the water stored in outer elastic cells

163    constitutes the only capacitive water source; water release from the xylem parenchyma and cavitated

164    conduits is neglected by this model. Sap flow ($F_{STEM}$) integrates the axial water flow through the xylem

165    compartment via root water uptake ($f_X$) and the radial water exchange between xylem and storage

166    compartment ($f_S$). Axial water flow ($f_X$) is calculated as the water potential gradient between the roots

167    and the stem divided by $R_X$, and radial water flow ($f_S$) is calculated as the first derivative defining the

168    change in water content of the storage compartment, which is influenced by the resistance to radial

169    flow between xylem and storage compartment ($R_S$, MPa h $g^{-1}$). The model equations are shown in the

170    supplementary material (Note S1). When transpiration starts, a water potential gradient between

171    xylem and storage compartment ($\Psi_X$ - $\Psi_S$) leads to radial flow from outer cells to the xylem to fulfill

172    the transpiration need; $\Psi_X$ is inferred from $\Psi_{LEAF}$ measurements (see below), whereas $\Psi_S$ is estimated

173    as a function of the water content and capacitance of the storage compartment (see Note S1). Water

174    depletion in the morning results in reduction in cell turgor and reversible stem shrinkage. Conversely,

175    water refilling in the afternoon, when atmospheric vapor pressure deficit and transpiration start to

176    decline, results in reversible stem swelling. Water potential in the storage compartment is the

177    algebraic sum of the osmotic potential ($\Psi_S^O$) and the turgor pressure ($\Psi_S^P$). Irreversible stem growth

178    occurs when carbon requirements are met (Daudet *et al.*, 2005) and turgor pressure exceeds a

179    threshold value for cell wall yielding (Γ, Lockhart 1965). For a detailed explanation of the principles of

180    the model see Steppe *et al.* (2006, 2008a) and De Pauw *et al.* (2008).

181    To allow variation in xylem hydraulic resistance of the root−to−leaf continuum ($R_X$, MPa h $g^{-1}$) and

182    stem hydraulic capacitance ($C_S$, g $MPa^{-1}$), the model was further developed by implementing two

183    equations and their corresponding parameters:

184 The hydraulic resistance was described to vary exponentially with $\Psi_{PD}$ (Baert *et al.*, 2015), which

185 accounted for day to day variations in $R_X$ with soil drying while assuming no daily refilling of cavitated

186 xylem:

187 $$R_X = r_1\, e^{(\Psi_{PD}^2)\, r_2} \qquad\qquad \text{Eqn. 1}$$

188 where $r_1$ (MPa h g$^{-1}$) and $r_2$ (MPa$^{-2}$) are the proportionality parameters influenced by plant

189 characteristics.

190 The hydraulic capacitance of the stem was calculated as the derivative of the water release curve

191 (Steppe *et al.*, 2006):

192 $$C_S = \frac{dW}{d\Psi} \qquad\qquad \text{Eqn. 2}$$

193 where dW is the variation in water content in the storage compartment (g h$^{-1}$) and d$\Psi$ the

194 corresponding variation in $\Psi$ (MPa h$^{-1}$). In this study, the cumulative water (W) release curve was

195 defined by a logarithmic equation of similar shape to those previously reported (e.g. Meinzer *et al.*,

196 2003, 2009; McCulloh *et al.*, 2014):

197 $$W = -log_{w_1}(w_2\Psi + 1) \qquad\qquad \text{Eqn. 3}$$

198 where $w_1$ and $w_2$ are the parameters defining the shape of the water release curve. The derived form

199 of Eqn. 3 results in an inverse equation between $C_S$ and $\Psi_{PD}$:

200 $$C_S = \frac{1}{(c_1\, \Psi_{PD} + c_2)} \qquad\qquad \text{Eqn. 4}$$

201 where $c_1$ (g$^{-1}$) and $c_2$ (MPa g$^{-1}$) are the proportionality parameters dependent on plant properties,

202 which are related to the parameters defining the water release curve (Eqn. 3) as follows: $w_1 = e^{c_1}$,

203 and $w_2 = \frac{\ln(w_1)}{c_2}$. Note that the purpose of this study is to evaluate seasonality in $R_X$ and $C_S$.

204 Therefore, $R_X$ and $C_S$ in this model fluctuates on a daily basis with $\Psi_{PD}$, so that both are assumed

205 constant within 24 h periods as diel variability in $R_X$ and $C_S$ is expected to be comparatively negligible

206 (see Baert *et al.*, 2015).

207    Four models were calibrated for each tree: [1] $R_X$ and $C_S$ were assumed to be constant (the simplest

208    framework, used for model calibration of $R_X$ and $C_S$), [2] $R_X$ was allowed to vary and $C_S$ was assumed

209    to be constant (model calibration of $r_1$, $r_2$ and $C_S$), [3] $C_S$ was allowed to vary and $R_X$ was assumed to

210    be constant (model calibration of $R_X$, $c_1$ and $c_2$), and [4] both $R_X$ and $C_S$ were allowed to vary (model

211    calibration of $r_1$, $r_2$, $c_1$ and $c_2$).  The resistance to radial flow between xylem and storage compartment

212    ($R_S$) was also calibrated in each model.

213    **2.3.2 Model simulation, calibration, and identifiability analyses**

214    Model simulations, calibrations and identifiability analyses were performed using the plant modelling

215    software PhytoSim (version 2.1, Phyto-IT, Mariakerke, Belgium). Simulations were conducted with a

216    fourth order variable step size solver of an accuracy of $10^{-6}$ and a maximum step size of 1 h.

217    Calibrations were done using the simplex method to minimize the weighted sum of squared errors

218    (SSE) for $\Delta D$ and $\Psi_X$. Identifiability analyses were performed to check whether the subset of model

219    parameters to calibrate was not correlated and sensitive enough, and thus was identifiable (De Pauw

220    *et al.*, 2008). A collinearity index (CI) above 15 indicated an unidentifiable subset of parameters.

221    Values of non-calibrated model parameters were directly measured or assigned from literature

222    (Table S1 in supplementary material).

223    Predawn water potential and $F_{STEM}$ were used as model inputs, and $\Delta D$ and $\Psi_X$ were used for

224    calibration purposes. The best model was selected using the final predicted error (FPE) criteria

225    (Steppe *et al.*, 2006):

226    $$FPE = \frac{SSE}{N} + \frac{2pSSE}{(N-p)\,N} \qquad\qquad \text{Eqn. 5}$$

227    where SSE is the weighted sum of squared errors for $\Delta D$ and $\Psi_X$, *N* is the number of observations,

228    and *p* the number of calibrated parameters. The first term of the FPE evaluates the goodness of fit

229    between measured and simulated data, whereas the second term penalizes over-parameterized

230    models. Thus, the smaller the FPE value, the better the model.

231    Because rain events and tree trembling resulted in irregular signals recorded by the automatic band

232    dendrometers, data was manually inspected to select a set of days that displayed reliable diel

233    patterns, i.e., smooth morning shrinkage and afternoon swelling. As the number of $\Delta D$ observations

234    after manual inspection differed among trees, FPE values also differed. To remove any effect

235    associated to the number of observations, values of FPE were normalized relative to the simplest

236    framework (constant $R_X$ and $C_S$) for each tree.

237    Models were calibrated under wet and dry conditions. As stem growth during the summer season is

238    limited by soil water availability in the surveyed site (Lempereur *et al.*, 2015), wet and dry periods

239    were defined according to growing or non-growing conditions, respectively. Periods that cover two

240    consecutive midday $\Psi_{LEAF}$ measurements were initially considered for model calibration: DOYs 113-

241    177 were selected for the wet period (spring and early summer) and DOYs 207-235 for the dry period

242    (late summer). Inaccurate simulations were initially obtained during the wet period and further

243    attempts to improve simulations were tested. First, the stem growth curve was adjusted to a

244    Gompertz-shaped curve (Winsor, 1932) to smooth large fluctuations registered by the band

245    dendrometers (Fig. 1D); and second, a shorter time period around a single $\Psi_{LEAF}$ measurement

246    campaign (DOY 176, early summer) was additionally examined.

247    To calibrate the models, midday $\Psi_X$ was inferred from midday $\Psi_{LEAF}$ measurements. Under dry

248    conditions, measurements of midday $\Psi_{LEAF}$ could be used as a surrogate of midday $\Psi_X$, because of the

249    strong stomatal limitation observed in the monitored trees (see Fig. 3 in Limousin *et al.*, 2010b)

250    which minimized the disequilibrium in water potential between xylem and leaves (Meinzer *et al.*,

251    2009). In contrast, substantial disequilibrium between midday $\Psi_{LEAF}$ and midday $\Psi_X$ might occur

252    when water is not limiting, as has been observed in *Q. ilex* seedlings (Rodríguez-Calcerrada *et al.*,

253    2017) and in Neotropical savanna trees (see Fig. 2 in Scholz *et al.*, 2007). Under wet conditions, the

254    difference between midday and predawn $\Psi_X$ ($\Delta\Psi_X$ = midday $\Psi_X$ − predawn $\Psi_X$) was assumed as a

255    constant fraction of $\Delta\Psi_{LEAF}$ ($\Delta\Psi_{LEAF}$ = midday $\Psi_{LEAF}$ − predawn $\Psi_{LEAF}$). The ratio $\Delta\Psi_X$ / $\Delta\Psi_{LEAF}$ was

256    obtained from measurements performed in *Q. ilex* seedlings ($\Delta\Psi_X$ / $\Delta\Psi_{LEAF}$ = 0.342; Fig. S1 in

257     supplementary material), in which leaves were covered with aluminium foil for one hour to measure

258     $\Psi_X$. Midday $\Psi_X$ was therefore estimated as a function of $\Psi_{PD}$ and $\Delta\Psi_{LEAF}$ (midday $\Psi_X = \Psi_{PD} + 0.342$ *

259     $\Delta\Psi_{LEAF}$). By using this approximation of $\Psi_X$, we made the assumptions that leaf hydraulic resistance

260     was a constant fraction of the tree hydraulic resistance independently of tree size (Sack *et al.*, 2003),

261     that the water potential difference between leaves and stem depended mainly on leaf transpiration,

262     and that the $\Psi_X$ difference between the trunk and the branches was negligible.

**2.4 Stem water refilling measurements**

264     Stem water refilling was estimated by integrating sap flow over intense rain events at the end of

265     summer drought. We only considered short (< 4 hours) and heavy (> 20 mm) rainfall events occurring

266     at night or in the late evening to ensure that recorded sap flow could be attributed to stem water

267     refilling and not to leaf transpiration (Betsch *et al.*, 2011), and to avoid rainfall events that resulted in

268     slow refilling extending beyond night-time. Sap flow was integrated along the rain event and

269     following night-time hours to estimate the volume of water refilled. Stem water refilling was then

270     divided by the corresponding shift in $\Psi_{PD}$ measured before and after the rain event to estimate $C_S$

271     (Eqn. 2) and compare it with values obtained from model simulations. Available measurements of

272     $\Psi_{PD}$ obtained less than one week before and after the rainfall event were necessary to calculate $C_S$.

273     As the first heavy rain in 2009 did not meet these requirements, different years were inspected and

274     suitable rain events were found in 2006 and 2007 to estimate $C_S$. TREE4 was excluded from this

275     analysis, as it was not monitored in 2006 and 2007. However, eighteen *Q. ilex* trees located in the

276     study site and equipped with thermal dissipation probes were additionally included.

**2.5 Data analyses**

278     To compare model performance (i.e. normalized FPE) among the four tested models and the two

279     surveyed periods, Tukey´s multiple comparison tests were performed using the *TukeyHSD* function in

280     the R software (version 3.2.3). The best model was then selected to obtain $R_X$ and $C_S$ along the

281     gradient of $\Psi_{PD}$ on a per-tree basis. To test whether $F_{STEM}$ and radial water flow ($f_S$) varied with $\Psi_{PD}$,

282 mixed models were adjusted using the *lme* function in the nlme library, in which stem was

283 considered as a random factor (n = 6). As the model output for $C_S$ refers to the whole tree, $C_S$ was

284 standardized per unit of storage volume. The storage volume was estimated as the product of stem

285 height by stem basal area subtracting the xylem compartment. The integrated root−to−leaf hydraulic

286 conductance was calculated as the inverse of the integrated root−to−leaf hydraulic resistance ($K_X$ =

287 $1/R_X$, g MPa$^{-1}$ h$^{-1}$). Predawn water potential causing 50% loss of $K_X$ ($\Psi_{50}$) was obtained following Baert

288 *et al.* (2015). To obtain the mean curve and confidence intervals of $C_S$, cumulative water release, and

289 integrated root−to−leaf $R_X$ and $K_X$ along the gradient of $\Psi_{PD}$, uncertainty analyses were performed in

290 PhytoSim using the averaged parameters among the six studied trees yielded by the best model. All

291 values presented in the text are means ± SE.

292 **3 Results**

293 Averaged among the six surveyed stems and across the whole year, daily sap flow was 4.11 ± 0.81 kg

294 day$^{-1}$ (Fig. 1C, Table 1), and mean annual diameter increment was 0.53 ± 0.20 mm year$^{-1}$ (Fig. 1D,

295 Table 1). During spring and early summer (DOYs 113-177), average temperature was 18.2 $^{o}$C and

296 accumulated rainfall 107.2 mm. Late summer was hot and dry, with an average temperature of 25.2

297 $^{o}$C and an accumulated rainfall of 11.8 mm during the dry modelled period (DOYs 207-235). The

298 lowest $\Psi_{LEAF}$ was measured at the end of this period, when it reached mean values of -3.3 MPa at

299 predawn and -3.9 MPa at midday (Fig. 1B).

300 Four models with constant or variable $R_X$ and $C_S$ were adjusted per tree and period to simulate ΔD

301 and $\Psi_X$ over time. A consistent pattern was observed under wet (Fig. 2A) and dry (Fig. 2B) conditions.

302 Relative to the simplest model (constant $R_X$ and $C_S$), the normalized FPE was not reduced when $R_X$

303 alone was allowed to vary (P > 0.1). In contrast, the normalized FPE was reduced (P < 0.001) when $C_S$

304 was allowed to vary with $\Psi_{PD}$. The model with variable $R_X$ and $C_S$ showed the lowest normalized FPE,

305 although its value did not differ significantly from that obtained with constant $R_X$ and variable $C_S$ (P >

306 0.1). Therefore, calibration of the model with a variable $C_S$ was the main improvement required to

307 accurately simulate $\Delta D$ and $\Psi_X$. Only data yielded by the best model (variable $R_X$ and $C_S$) is shown

308 hereafter.

309 Models were calibrated under wet and dry conditions. Only TREE5 was not modelled during the wet

310 season due to the inconsistent dendrometer signal at the time of $\Psi_{LEAF}$ measurement. Because of

311 concurrent stem growth, inaccurate simulations of $\Delta D$ were initially obtained during the wet period

312 when considering long temporal spans (DOYs 113-177; data not shown). Shorter temporal spans of 3-

313 4 days resulted in realistic simulations of $\Psi_X$ and $\Delta D$ (Fig. 3A-C, FPE = 6.04 ± 1.90). The length of the

314 simulation period was not an issue under dry conditions when stem growth was impeded, and

315 accurate simulations were obtained for every tree throughout the one-month simulated period (Fig.

316 3D-F, FPE = 7.71 ± 2.11). During the wet season, cell turgor pressure at night-time was higher than

317 the turgor threshold for cell wall yielding ($\Psi_S^P > \Gamma$, Fig. 3A) leading to irreversible stem growth (Fig.

318 3B). During the dry season, soil drying progressively reduced $\Psi_X$, $\Psi_S$ and cell osmotic potential, which

319 explained the rather constant pattern of cell turgor pressure, which was below the turgor threshold

320 for cell wall yielding ($\Psi_S^P < \Gamma$, Fig. 3D), thus impeding irreversible stem growth (Fig. 3E). Morning stem

321 shrinkage and afternoon stem swelling (Fig. 3B, 3E) were caused by the radial water flow between

322 xylem and storage compartments ($f_S$, Fig. 3C, 3F).

323 Daily $F_{STEM}$ was directly related to $\Psi_{PD}$ in every surveyed stem (P < 0.01, Fig. 4A). Averaged among the

324 six stems, $F_{STEM}$ decreased from 7.50 ± 0.83 kg day$^{-1}$ during the wet period ($\Psi_{PD}$ = -1.0 MPa) to 1.46 ±

325 0.81 kg day$^{-1}$ at the end of the dry period ($\Psi_{PD}$ = -3.3 MPa, P < 0.001). The decrease in daily stem

326 water release from the storage to the xylem compartment (daily sum of negative $f_S$, hereafter daily

327 $|f_S|$, in kg day$^{-1}$) with $\Psi_{PD}$ was significant in only half of the surveyed trees (P < 0.05, Fig. 4B) and

328 became non-significant when pooling trees across a range of $\Psi_{PD}$ from -1.0 to -3.3 MPa (P = 0.15).

329 Considering the dry period only, daily $|f_S|$ significantly decreased with $\Psi_{PD}$ (P < 0.001) from 0.13 ±

330 0.03 to 0.10 ± 0.03 kg day$^{-1}$ for a corresponding reduction in $\Psi_{PD}$ of 1.3 MPa (from -2.0 to -3.3 MPa).

331 Across the year, daily sap flow was reduced to a greater extent than daily $|f_S|$ as the soil dried out.

332    Hence, the daily contribution of $|f_S|$ to $F_{STEM}$ increased with drought severity (P < 0.001) from 2.0 ±

333    0.9 % to 5.1 ± 0.9 % when $\Psi_{PD}$ decreased from -1.0 to -3.3 MPa (Fig. 4C).

334    Stem hydraulic capacitance decreased with drought stress. Mean $C_S$ on a storage volume basis was

335    61.69 ± 6.30 kg MPa$^{-1}$ m$^{-3}$ under wet conditions (Table 2) and reached lowest values of 24.93 ± 4.14

336    kg MPa$^{-1}$ m$^{-3}$ at the end of the summer drought (Table 3). Fig. 5A illustrates the mean cumulative

337    release of water from storage compartments and the change in $C_S$ at the tree level obtained in the

338    dry period and extrapolated to a wider range of $\Psi_{PD}$. Hydraulic capacitance obtained from model

339    calibration during the wet period ($C_S$ = 314.51 ± 38.83 g MPa$^{-1}$ tree$^{-1}$) was underestimated by the $C_S$

340    curve extrapolated from the dry period.  Similarly, Fig. 5B displays mean $R_X$ and $K_X$ curves obtained in

341    the dry period. The vulnerability curve of root–to–leaf hydraulic conductance obtained from the dry

342    period showed a mean $\Psi_{50}$ value of -2.67 ± 0.23 MPa (Table 3). The $R_X$ value obtained from direct

343    model calibration under wet conditions (5.01 ± 0.45 × 10$^{-4}$ MPa h g$^{-1}$, Table 2) was overestimated by

344    the $R_X$ curve extrapolated from summer drought.

345    Two rain events were used to independently estimate $C_S$ from stem water refilling. In 2006, 24 mm of

346    rainfall were registered during the night of DOY 228 to 229, whereas in 2007, a stronger rainfall of

347    75.5 mm occurred in the night of DOY 261 to 262. The corresponding mean increase in $\Psi_{PD}$ was 2.6

348    and 2.9 MPa for 2006 and 2007, respectively. Stem water refilling and $C_S$ on a tree basis were

349    exponentially related to stem size across the 23 trees examined (P < 0.001; Fig. 6). Average stem

350    water refilling and $C_S$ among the five trees monitored in both approaches were 1134 ± 149 g tree$^{-1}$

351    and 414 ± 45 g MPa$^{-1}$ tree$^{-1}$, respectively.

352    **4 Discussion**

353    **4.1 The importance of a variable hydraulic capacitance in tree modelling**

354    Hydraulic capacitance is commonly measured as the slope of the initial and nearly linear portion of

355    the curve between the cumulative water release and water potential (Meinzer *et al.*, 2003, 2008;

356    Barnard *et al.*, 2011; McCulloh *et al.*, 2014). These estimates of $C_S$ are therefore obtained within the

357 range of $\Psi_X$ when plants are not subjected to drought stress. Notwithstanding, $C_S$ varies seasonally as

358 water storage refilling is limited by soil drying (Verbeeck et al., 2007; Scholz et al., 2008; Steppe et al.,

359 2008b; Kocher et al., 2013; Matheny et al., 2015). Progressive decoupling between daily capacitive

360 water discharge and daily water refilling leads to water reserves depletion, and accordingly, a net

361 reduction in stem diameter is commonly observed during the dry season (Fig. 3E; Zweifel et al., 2000;

362 Lempereur et al., 2015). Progressive depletion of water reservoirs should be incorporated in process-

363 based hydraulic models by the implementation of a direct relationship between $C_S$ and soil water

364 availability. However, to the best of our knowledge, no mechanistic model has yet considered

365 drought-induced variability in $C_S$ to model tree hydraulic functioning. Furthermore, and unexpectedly,

366 considering the variation of $C_S$ with $\Psi_{PD}$ was also found to result in more accurate simulations of $\Psi_X$

367 and $\Delta D$ during the wet period. In contrast to previous studies using this model in which $C_S$ was

368 assumed constant under well-watered regimes and stable soil water content (e.g. Steppe et al., 2006,

369 2008a; De Schepper & Steppe, 2010), considering a variable $C_S$ was here necessary to simulate the

370 increase in turgor that yielded irreversible cell wall extension. Assuming a constant $C_S$ in our study

371 resulted in a progressive reduction of maximum daily turgor pressure that impeded stem growth

372 (simulations not shown) as $\Psi_{PD}$ slightly declined during this "wet" period (Fig. 3A). Consequently,

373 under both wet and dry conditions, assumptions of constant $C_S$ may partially explain why tree models

374 fail to reproduce variations in diameter and $\Psi_X$ in environments where soil water availability

375 fluctuates. We suggest that to better predict and understand tree hydraulic functioning and the risk

376 of hydraulic failure in dry regions, it is necessary to take into account the dynamic nature of $C_S$.

377 Because $C_S$ is commonly measured under moist conditions, estimates of $C_S$ on a storage volume basis

378 in early summer (62 kg m$^{-3}$ MPa$^{-1}$, Table 2) might be more appropriate for literature comparison.

379 Hydraulic capacitance of Q. ilex at this time of year was consistent with the reported range for

380 evergreen sclerophyll species (6-102 kg m$^{-3}$ MPa$^{-1}$, Richards et al. 2014) and lower than the ones for

381 tropical species (70-420 kg m$^{-3}$ MPa$^{-1}$, Meinzer et al. 2003, 2009) and conifers (107-886 kg m$^{-3}$ MPa$^{-1}$,

382 Barnard et al. 2011, McCulloh et al. 2014). Nevertheless, neglecting the xylem tissues as capacitive

383    water sources might lead to underestimation of the overall hydraulic capacitance of *Q. ilex* stems in

384    our study (see below). Hydraulic capacitance decreased across the season from 62 to 25 kg m$^{-3}$ MPa$^{-1}$

385    (from DOY 176 to 235, respectively). The 60% reduction in $C_S$ illustrates the importance of

386    implementing variable $C_S$ in mechanistic models to accurately simulate tree water status and

387    diameter variations. Our modelling approach further allowed estimation of the daily contribution of

388    internal water storage to total daily sap flow ($|f_S|$ / $F_{STEM}$) as a function of $\Psi_{PD}$. The average $|f_S|$ /

389    $F_{STEM}$ ratio ranged between 2% in early summer and 5% at the end of summer drought when $\Psi_{PD}$

390    reached mean values of − 3.3 MPa (Fig. 4C). This ratio is at the lower end of observations made in

391    other species that may reach up to 19% when only elastic tissues are considered (see Table 3 in

392    Betsch *et al.*, 2011). The low reliance on stored water to maintain transpiration rates in *Q. ilex* might

393    be related to the wood features of this species with relatively high wood density and small vessel size

394    (Limousin *et al.*, 2010a). These characteristics make trees more cavitation-resistant to xylem tension,

395    an adaptation which seems to be related to a limited capacity to reduce xylem tension via radial

396    water release (Meinzer *et al.*, 2008, 2009; Richards *et al.*, 2014). This trade-off also explains that $C_S$ of

397    *Q. ilex* is at the lower end of reported values (see Fig. 5 in Meinzer *et al.* 2009 for comparison).

398    Despite low $|f_S|$ / $F_{STEM}$ ratios, the reliance on stored water increased with drought stress due to a

399    more pronounced reduction in daily $F_{STEM}$ compared to daily $|f_S|$. A similar pattern was also noticed

400    in *Quercus robur* L., which used stored water primarily when subjected to drought stress (Matheny *et*

401    *al.*, 2015). These observations suggest greater relevance of stem water reservoirs to maintain

402    transpiration rates and tree hydraulic integrity in future drier climates (see Tyree & Ewers 1991; and

403    Bréda *et al.* 2006).

404    **4.2 Model limitations**

405    Two limitations related to the model structure and assumptions were detected during this study.

406    First, accurate simulations of diameter variations during the wet period were restricted to time

407    frames of 3-4 days. Beyond this short time interval, diameter simulations progressively deviated from

408    measured values. During dry conditions, however, the length of the model period was not an issue

409 because irreversible stem growth was prevented by soil water limitation (Lempereur *et al.*, 2015).

410 Any diameter variation during summer drought could be uniquely ascribed to radial water flow

411 causing elastic stem shrinkage and swelling. In contrast, during the wet period when irreversible

412 growth occurred, the carbon status of the plant is a factor involved in growth, for example via

413 osmotic regulation of cell turgor and elongation (Lockhart, 1965; Daudet *et al.*, 2005). The lack of

414 carbon-related equations in our water-based model describing sugar transport and/or carbon

415 allocation to growth could explain inaccurate simulations when the modelled period extended

416 beyond 3-4 days. Accordingly, the generally prescribed time frame for this model ranges from one

417 day to two weeks (Steppe *et al.*, 2006, 2008b). More sophisticated models integrating water and

418 carbon transport processes should be further developed to simulate irreversible stem growth on a

419 seasonal basis (De Schepper & Steppe, 2010; Mencuccini *et al.*, 2015; Steppe *et al.*, 2015a).

420 Second, the model is theoretically designed to estimate $C_S$ only for outer tissues and we ignore the

421 amount of water released by the xylem compartment. The contribution of the xylem to whole stem

422 diameter variations is expected to be minor (Zweifel *et al.*, 2000; Steppe & Lemeur, 2004; Steppe *et*

423 *al.*, 2006), and our model therefore assumes the xylem as a rigid compartment and outer tissues −

424 namely cambium, phloem, and phelloderm − as an elastic storage compartment responsible for diel

425 shrinkage and swelling. Nevertheless, the amount of water released for a given change in volume is

426 higher in the xylem than in the outer tissues; about 3.5 times higher in the case of savanna trees,

427 which results in a greater capacitance of the xylem compartment (Scholz *et al.*, 2007, 2008). Higher

428 capacitance of the xylem can be ascribed to both elastic living parenchyma and the capacitive effect

429 of cavitated conduits (Tyree & Ewers, 1991; Hölttä *et al.*, 2009; Richards *et al.*, 2014). Thus, water

430 release from the xylem could be important in large trees with a high proportion of sapwood and

431 lumen volume (Waring *et al.*, 1979; Hölttä *et al.*, 2009; Betsch *et al.*, 2011) or with large and

432 numerous sapwood parenchyma rays such as *Q. ilex*. Models considering the capacitive effect of

433 cavitation (Hölttä *et al.*, 2009) and the xylem as an elastic compartment with a distinct elastic bulk

434 modulus and hydraulic capacitance (Perämäki *et al.*, 2005) would be necessary to further disentangle

435    the contribution of elastic outer tissues and xylem parenchyma, and inelastic cavitated conduits to

436    the overall capacitive discharge of water to the transpiration stream.

437    **4.3 Simulated stem water release curves, root–to–leaf vulnerability curves and model validation**

438    Simulations performed under dry conditions misestimated both $C_S$ and $R_X$ when extrapolated to a

439    wider range of $\Psi_{PD}$ during wet conditions, and values obtained for well-watered conditions were also

440    necessary to realistically describe the $C_S$ and $R_X$ curves over the entire $\Psi_{PD}$ range (Fig. 5). This

441    observation denotes that any extrapolation beyond the surveyed range of $\Psi_{PD}$ must be taken with

442    caution. More frequent measurements of $\Psi_{LEAF}$ (or $\Psi_X$) would be necessary to re-calibrate model

443    parameters at a higher temporal resolution (Steppe *et al.*, 2008b) and obtain a more accurate

444    evolution of $C_S$ and $R_X$ across a wider range of $\Psi_{PD}$.

445    Estimates of stem water refilling following first heavy rains at the end of the drought period and the

446    vulnerability curves obtained by measurements at the organ scale were compared to model

447    simulations. At the end of summer drought, the modelled cumulative water release averaged 683 g

448    tree$^{-1}$ at a $\Psi_{PD}$ of -3.33 MPa (Fig. 5A), which is 60% of that estimated from the refilling calculations

449    (1134 g tree$^{-1}$ for a corresponding increase in $\Psi_{PD}$ of 2.75 MPa, Fig. 6A). Likewise, mean $C_S$ modelled

450    across the range of surveyed conditions (from 103 to 314 g MPa$^{-1}$ tree$^{-1}$, Fig. 5A) was lower than that

451    estimated following heavy rains (414 g MPa$^{-1}$ tree$^{-1}$, Fig. 6B). Inaccurate assumptions to estimate

452    stem storage capacity and $C_S$ using both approaches may account for this difference. First, $C_S$ could

453    be overestimated from water refilling calculations because the corresponding water potential

454    increase was measured several days apart from the refilling event, and was therefore slightly

455    underestimated. Besides, water refilling of branches and leaves incorrectly attributed to the stem

456    may overestimate the actual stem storage capacity. Second, $C_S$ might be underestimated from model

457    simulations due to the water release from xylem tissues (Scholz *et al.*, 2008; Hölttä *et al.*, 2009)

458    undetected by our model. Models that integrate the hydraulic capacitance of the xylem

459    compartment, continuous *in vivo* measurements of wood water content using frequency domain

460 reflectometry (Matheny *et al.*, 2015), or destructive sampling to obtain stem moisture release curves

461 with psychrometers (Meinzer *et al.*, 2003) might be complementary approaches to more accurately

462 estimate the overall hydraulic capacitance of the stem. Likewise, direct measurements of $\Psi_X$ would

463 result in more accurate estimates of $C_S$ than the simulated here, in which $\Psi_X$ was inferred from $\Psi_{LEAF}$

464 measurements.

465 On the other hand, variation in $R_X$ as a function of drought stress affected to a lesser extent the

466 model performance. The simulated vulnerability curve along the root–to–leaf continuum exhibited

467 reasonable agreement with measurements made at the organ scale at the same site. The mean

468 simulated $\Psi_{50}$ was -2.67 MPa (Table 3). Estimates of $\Psi_{50}$ in excised branches and roots of *Q. ilex* trees

469 located at the same site averaged -3.88 and -2.39 MPa, respectively, using the air injection technique

470 after flushing native embolism (Limousin *et al.*, 2010a), and -4.7 MPa in branches using the bench

471 drying technique (Martin-StPaul *et al.* 2014). Vulnerability to drought in the root–to–leaf continuum

472 is determined to the greatest extent by the most vulnerable node along this hydraulic pathway (Baert

473 *et al.*, 2015). In this particular case, roots might be the major constrain to water flow along the root–

474 to–leaf continuum, followed by stems and branches (Tyree & Ewers, 1991; Sperry & Love, 2015).

475 Therefore, the integrated $\Psi_{50}$ (-2.67 MPa) might primarily reflect the hydraulic vulnerability of roots.

476 This alternative approach to generate integrated root–to–leaf vulnerability curves might be useful to

477 describe the hydraulic functioning of the whole tree while avoiding to separately measure multiple

478 hydraulic resistances (Baert *et al.*, 2015), which might be controversial due to the strong variability in

479 hydraulic conductance ascribed to methodological issues (Cochard & Delzon, 2013; Martin-StPaul *et*

480 *al.*, 2014).

**References**

Baert A, De Schepper V, Steppe K (2015) Variable hydraulic resistances and their impact on plant drought response modelling. *Tree Physiology*, **35**, 439–449.

Barnard DM, Meinzer FC, Lachenbruch B, McCulloh KA, Johnson DM, Woodruff DR (2011) Climate-related trends in sapwood biophysical properties in two conifers: avoidance of hydraulic dysfunction through coordinated adjustments in xylem efficiency, safety and capacitance. *Plant, Cell & Environment*, **34**, 643–654.

Betsch P, Bonal D, Breda N, Montpied P, Peiffer M, Tuzet A, Granier A (2011) Drought effects on water relations in beech: The contribution of exchangeable water reservoirs. *Agricultural and Forest Meteorology*, **151**, 531–543.

Bréda N, Huc R, Granier A, Dreyer E (2006) Temperate forest trees and stands under severe drought: a review of ecophysiological responses, adaptation processes and long-term consequences. *Annals of Forest Science*, **63**, 625–644.

Brodersen CR, McElrone AJ (2013) Maintenance of xylem network transport capacity: a review of embolism repair in vascular plants. *Frontiers in Plant Science*, **4**, 108.

Campbell GS (1974) A simple method for determining unsaturaed conductivity from moisture retention data. *Soil Science*, **117**, 311–314.

509    Choat B, Jansen S, Brodribb TJ et al. (2012) Global convergence in the vulnerability of forests to

510        drought. *Nature*, **491**, 752–5.

511    Cochard H, Delzon S (2013) Hydraulic failure and repair are not routine in trees. *Annals of Forest*

512        *Science*, **70**, 659–661.

513    Daudet F-A, Améglio T, Cochard H, Archilla O, Lacointe A (2005) Experimental analysis of the role of

514        water and carbon in tree stem diameter variations. *Journal of Experimental Botany*, **56**, 135–44.

515    Epila J, De Baerdemaeker NJF, Vergeynst LL, Maes WH, Beeckman H, Steppe K (2017) Capacitive

516        water release and internal leaf water relocation delay drought-induced cavitation in African

517        Maesopsis eminii. *Tree Physiology*, DOI: 10.1093/treephys/tpw128.

518    Goldstein G, Andrade JL, Meinzer FC, Holbrook NM, Cavelier J, Jackson P, Celis A (1998) Stem water

519        storage and diurnal patterns of water use in tropical forest canopy trees. *Plant, Cell &*

520        *Environment*, **21**, 397–406.

521    Granier A (1985) Une nouvelle méthode pour la mesure du flux de sève brute dans le tronc des

522        arbres. *Annals of Forest Science*, **42**, 193–200.

523    Hölttä T, Cochard H, Nikimaa E, Mencuccini M (2009) Capacitive effect of cavitation in xylem

524        conduits: results from a dynamic model. *Plant, Cell & Environment*, **32**, 10–21.

525    Kocher P, Horna V, Leuschner C (2013) Stem water storage in five coexisting temperate broad-leaved

526        tree species: significance, temporal dynamics and dependence on tree functional traits. *Tree*

527        *Physiology*, **33**, 817–832.

528    Lempereur M, Martin-StPaul NK, Damesin C, Joffre R, Ourcival J-M, Rocheteau A, Rambal S (2015)

529        Growth duration is a better predictor of stem increment than carbon supply in a Mediterranean

530        oak forest: implications for assessing forest productivity under climate change. *New Phytologist*,

531        **207**, 579–590.

532    Limousin JM, Rambal S, Ourcival JM, Rocheteau A, Joffre R, Rodriguez-Cortina R (2009) Long-term

533     transpiration change with rainfall decline in a Mediterranean Quercus ilex forest. *Global Change*

534     *Biology*, **15**, 2163–2175.

535     Limousin JM, Longepierre D, Huc R, Rambal S (2010a) Change in hydraulic traits of Mediterranean

536     *Quercus ilex* subjected to long-term throughfall exclusion. *Tree Physiology*, **30**, 1026–1036.

537     Limousin JM, Misson L, Lavoir AV, Martin NK, Rambal S (2010b) Do photosynthetic limitations of

538     evergreen Quercus ilex leaves change with long-term increased drought severity? *Plant, Cell &*

539     *Environment*, **33**, 863–875.

540     Lockhart JA (1965) An analysis of irreversible plant cell elongation. *Journal of Theoretical Biology*, **8**,

541     264–275.

542     Martin-StPaul NK, Longepierre D, Huc R et al. (2014) How reliable are methods to assess xylem

543     vulnerability to cavitation? The issue of "open vessel" artifact in oaks. *Tree Physiology*, **34**, 894–

544     905.

545     Matheny AM, Bohrer G, Garrity SR, Morin TH, Howard CJ, Vogel CS (2015) Observations of stem

546     water storage in trees of opposing hydraulic strategies. *Ecosphere*, **6**, 165.

547     McCulloh KA, Johnson DM, Meinzer FC, Woodruff DR (2014) The dynamic pipeline: hydraulic

548     capacitance and xylem hydraulic safety in four tall conifer species. *Plant, Cell & Environment*,

549     **37**, 1171–1183.

550     Meinzer FC, James SA, Goldstein G, Woodruff D (2003) Whole-tree water transport scales with

551     sapwood capacitance in tropical forest canopy trees. *Plant, Cell & Environment*, **26**, 1147–1155.

552     Meinzer FC, Woodruff DR, Domec J-C, Goldstein G, Campanello PI, Gatti MG, Villalobos-Vega R (2008)

553     Coordination of leaf and stem water transport properties in tropical forest trees. *Oecologia*,

554     **156**, 31–41.

555     Meinzer FC, Johnson DM, Lachenbruch B, McCulloh KA, Woodruff DR (2009) Xylem hydraulic safety

556     margins in woody plants: coordination of stomatal control of xylem tension with hydraulic

557 capacitance. *Functional Ecology*, **23**, 922–930.

558 Mencuccini M, Minunno F, Salmon Y, Martínez-Vilalta J, Hölttä T (2015) Coordination of physiological

559  traits involved in drought-induced mortality of woody plants. *New Phytologist*, **208**, 396–409.

560 Mouillot F, Rambal S, Lavorel S (2001) A generic process-based SImulator for meditERRanean

561  landscApes (SIERRA): design and validation exercises. *Forest Ecology and Management*, **147**,

562  75–97.

563 De Pauw DJW, Steppe K, De Baets B (2008) Identifiability analysis and improvement of a tree water

564  flow and storage model. *Mathematical Biosciences*, **211**, 314–332.

565 Perämäki M, Vesala T, Nikinmaa E (2005) Modeling the dynamics of pressure propagation and

566  diameter variation in tree sapwood. *Tree Physiology*, **25**, 1091–1099.

567 Rambal S, Ourcival J-M, Joffre R, Mouillot F, Nouvellon Y, Reichstein M, Rocheteau A (2003) Drought

568  controls over conductance and assimilation of a Mediterranean evergreen ecosystem: scaling

569  from leaf to canopy. *Global Change Biology*, **9**, 1813–1824.

570 Rambal S, Lempereur M, Limousin JM, Martin-StPaul NK, Ourcival JM, Rodríguez-Calcerrada J (2014)

571  How drought severity constrains gross primary production (GPP) and its partitioning among

572  carbon pools in a *Quercus ilex* coppice? *Biogeosciences*, **11**, 6855–6869.

573 Richards AE, Wright IJ, Lenz TI, Zanne AE (2014) Sapwood capacitance is greater in evergreen

574  sclerophyll species growing in high compared to low-rainfall environments. *Functional Ecology*,

575  **28**, 734–744.

576 Rodríguez-Calcerrada J, Li M, López R et al. (2017) Drought-induced shoot dieback starts with massive

577  root xylem embolism and variable depletion of nonstructural carbohydrates in seedlings of two

578  tree species. *New Phytologist*, **213**, 597–610.

579 Ruffault J, Martin-StPaul NK, Rambal S, Mouillot F (2013) Differential regional responses in drought

580  length, intensity and timing to recent climate changes in a Mediterranean forested ecosystem.

581      *Climatic Change*, **117**, 103–117.

582 Sack L, Cowan PD, Jaikumar N, Holbrook NM (2003) The "hydrology" of leaves: co-ordination of

583      structure and function in temperate woody species. *Plant, Cell and Environment*, **26**, 1343–

584      1356.

585 De Schepper V, Steppe K (2010) Development and verification of a water and sugar transport model

586      using measured stem diameter variations. *Journal of Experimental Botany*, **61**, 2083–2099.

587 Scholz FC, Bucci SJ, Goldstein G, Meinzer FC, Franco AC, Miralles-Wilhelm F (2007) Biophysical

588      properties and functional significance of stem water storage tissues in Neotropical savanna

589      trees. *Plant, Cell & Environment*, **30**, 236–248.

590 Scholz FC, Bucci SJ, Goldstein G, Meinzer FC, Franco AC, Miralles-Wilhelm F (2008) Temporal

591      dynamics of stem expansion and contraction in savanna trees: withdrawal and recharge of

592      stored water. *Tree Physiology*, **28**, 469–480.

593 Sperry JS, Love DM (2015) What plant hydraulics can tell us about responses to climate-change

594      droughts. *New Phytologist*, **207**, 14–27.

595 Sperry JS, Adler FR, Campbell GS, Comstock JP (1998) Limitation of plant water use by rhizosphere

596      and xylem conductance: Results from a model. *Plant, Cell & Environment*, **21**, 347–359.

597 Steppe K, Lemeur R (2004) An experimental system for analysis of the dynamic sap-flow

598      characteristics in young trees: results of a beech tree. *Functional Plant Biology*, **31**, 83–92.

599 Steppe K, De Pauw DJW, Lemeur R, Vanrolleghem A (2006) A mathematical model linking tree sap

600      flow dynamics to daily stem diameter fluctuations and radial stem growth. *Tree Pysiology*, **26**,

601      257–273.

602 Steppe K, De Pauw DJW, Lemeur R (2008a) A step towards new irrigation scheduling strategies using

603      plant-based measurements and mathematical modelling. *Irrigation Science*, **26**, 505–517.

604 Steppe K, De Pauw DJW, Lemeur R (2008b) Validation of a dynamic stem diameter variation model

605    and the resulting seasonal changes in calibrated parameter values. *Ecological Modelling*, **218**,

606    247–259.

607    Steppe K, Cochard H, Lacointe A, Améglio T (2012) Could rapid diameter changes be facilitated by a

608    variable hydraulic conductance? *Plant, Cell & Environment*, **35**, 150–157.

609    Steppe K, Sterck F, Deslauriers A (2015a) Diel growth dynamics in tree stems: linking anatomy and

610    ecophysiology. *Trends in Plant Science*, **20**, 335–343.

611    Steppe K, Vandegehuchte MW, Tognetti R, Mencuccini M (2015b) Sap flow as a key trait in the

612    understanding of plant hydraulic functioning. *Tree Physiology*, **35**, 341–345.

613    De Swaef T, De Schepper V, Vandegehuchte MW, Steppe K (2015) Stem diameter variations as a

614    versatile research tool in ecophysiology. *Tree Physiology*, **35**, 1047–1061.

615    Tyree M, Ewers FW (1991) The hydraulic architecture of trees and other woody plants. *New*

616    *Phytologist*, **119**, 345–360.

617    Verbeeck H, Steppe K, Nadezhdina N et al. (2007) Atmospheric drivers of storage water use in Scots

618    pine. *Biogeosciences*, **4**, 657–671.

619    Waring RH, Whitehead D, Jarvis PG (1979) The contribution of stored water to transpiration in Scots

620    pine. *Plant, Cell & Environment*, **2**, 309–317.

621    Winsor CP (1932) The Gompertz curve as a growth curve. *Proceedings of the National Academy of*

622    *Sciences*, **18**, 1–8.

623    Zweifel R, Item H, Häsler R (2000) Stem radius changes and their relation to stored water in stems of

624    young Norway spruce trees. *Trees - Structure and Function*, **15**, 50–57.

625    Zweifel R, Steppe K, Sterck FJ (2007) Stomatal regulation by microclimate and tree water relations:

626    interpreting ecophysiological field data with a hydraulic plant model. *Journal of Experimental*

627    *Botany*, **58**, 2113–2131.

628 **Table 1.** Diameter at breast height (DBH), tree height, accumulated diameter increment and mean

629 daily sap flow during 2009 for the six monitored *Quercus ilex* trees.

| | DBH | Height | Annual diameter increment | Mean sap flow |
|---|---|---|---|---|
| | (cm) | (m) | (mm year$^{-1}$) | (kg day$^{-1}$) |
| TREE1 | 9.55 | 5.3 | 0.25 | 2.55 |
| TREE2 | 11.05 | 5.0 | 0.16 | 3.00 |
| TREE3 | 10.70 | 5.0 | 0.51 | 5.87 |
| TREE4 | 13.20 | 5.6 | 1.21 | 7.32 |
| TREE5 | 10.05 | 5.2 | -0.10 | 2.90 |
| TREE6 | 12.25 | 4.5 | 1.15 | 3.00 |

630 Tree DBH measured at the beginning of the 2009 growing season

631

632　**Table 2.** Hydraulic resistance to radial flow between the xylem and the storage compartment ($R_S$),

633　hydraulic resistance of the root–to–leaf segment ($R_X$), and stem hydraulic capacitance ($C_S$) obtained

634　from the mechanistic water flow and storage model describing the hydraulic functioning of *Quercus*

635　*ilex* trees during the wet season when stem growth occurred.

| | $R_s$ | $R_X$ | $C_S$ |
|---|---|---|---|
| | (MPa h g$^{-1}$) | (MPa h g$^{-1}$) | (kg MPa$^{-1}$ m$^{-3}$) |
| | $10^{-2}$ | $10^{-4}$ | |
| TREE1 | 0.97 | 4.59 [4.59 - 4.59] | 64.02 [54.66 – 72.22] |
| TREE2 | 1.41 | 5.72 [5.72 -5.72] | 50.06 [45.03 – 54.79] |
| TREE3 | 0.93 | 4.59 [4.59 -4.59] | 86.07 [73.33 – 98.28] |
| TREE4 | 0.53 | 3.65 [3.62 -3.69] | 61.38 [54.98 – 66.94] |
| TREE5[1] | NA | NA | NA |
| TREE6 | 1.15 | 6.49 [6.38 – 6.62] | 46.91 [41.67 – 52.69] |
| mean | 1.00 | 5.01 | 61.69 |
| (SE) | (0.13) | (0.45) | (6.30) |

636　$R_S$ was assumed constant whereas $R_X$ and $C_S$ were allowed to vary with predawn water potential (Eqn.

637　1 and Eqn. 4, respectively). The modelled period lasted 3-4 days and included DOY176, when leaf

638　water potential was measured. Mean values of $R_X$ and $C_S$ on a storage volume basis are shown;

639　minimum and maximum values for this period are indicated in square brackets.

640　[1] TREE5 was not modelled due to an inconsistent dendrometer signal.

641 **Table 3.** Calibrated parameters used in the mechanistic water flow and storage model describing the

642 hydraulic functioning of *Quercus ilex* trees during summer drought when stem growth was impeded.

643 The hydraulic resistance ($R_X$) and hydraulic capacitance ($C_S$) were allowed to vary with predawn water

644 potential ($\Psi_{PD}$). Estimates of $C_S$ and the $\Psi_{50}$ from the vulnerability curve were obtained from model

645 simulations.

| | Calibrated parameters[1] | | | | | $C_S$[2] | | $\Psi_{50}$[3] |
|---|---|---|---|---|---|---|---|---|
| | $R_s$ | $c_1$ | $c_2$ | $r_1$ | $r_2$ | DOY208 | DOY234 | |
| | (MPa h g$^{-1}$) | (g$^{-1}$) | (MPa g$^{-1}$) | (MPa h g$^{-1}$) | (MPa$^{-2}$) | (kg MPa$^{-1}$ m$^{-3}$) | | (MPa) |
| | $10^{-2}$ | $10^{-3}$ | $10^{-3}$ | $10^{-3}$ | $10^{-1}$ | | | |
| TREE1 | 1.95 | -3.07 | 2.68 | 0.99 | 1.29 | 26.52 | 18.48 | -2.32 |
| TREE2 | 1.73 | -2.54 | 2.01 | 1.68 | 0.67 | 28.91 | 19.84 | -3.21 |
| TREE3 | 2.30 | -2.33 | 2.78 | 1.26 | 1.53 | 31.75 | 23.34 | -2.13 |
| TREE4 | 0.53 | -0.73 | 1.11 | 0.77 | 0.91 | 56.30 | 45.30 | -2.76 |
| TREE5 | 1.31 | -2.99 | 1.20 | 3.15 | 1.55 | 37.43 | 22.66 | -2.12 |
| TREE6 | 1.88 | -2.28 | 2.34 | 3.67 | 0.58 | 28.04 | 19.96 | -3.46 |
| mean | 1.62 | -2.32 | 2.02 | 1.92 | 1.09 | 34.82 | 24.93 | -2.67 |
| (SE) | (0.25) | (0.35) | (0.29) | (0.49) | (0.17) | (4.57) | (4.14) | (0.23) |

646 [1] Five parameters were calibrated: the proportionality parameters $c_1$ and $c_2$ defining $C_S$ (Eqn. 4), the

647 proportionality parameters $r_1$ and $r_2$ defining $R_X$ (Eqn. 1), and the radial hydraulic resistance between

648 the xylem and the storage compartment ($R_S$).

649 [2] $C_S$ was estimated for two dates when $\Psi_{PD}$ was measured (DOYs 208 and 234) and calculated on a

650 storage volume basis.

651 [3] $\Psi_{50}$ is the $\Psi_{PD}$ causing 50% loss of maximum hydraulic conductance along the integrated

652 root−to−leaf continuum.

653

**Figure 1**. Daily air temperature and precipitation (A), soil water storage and predawn and midday leaf

655 water potential (means ± SE; B), daily sap flow (C), and daily stem diameter variations (D) during the

656 year 2009. Ecophysiological measurements were performed on six *Quercus ilex* trees of the

657 experimental site.
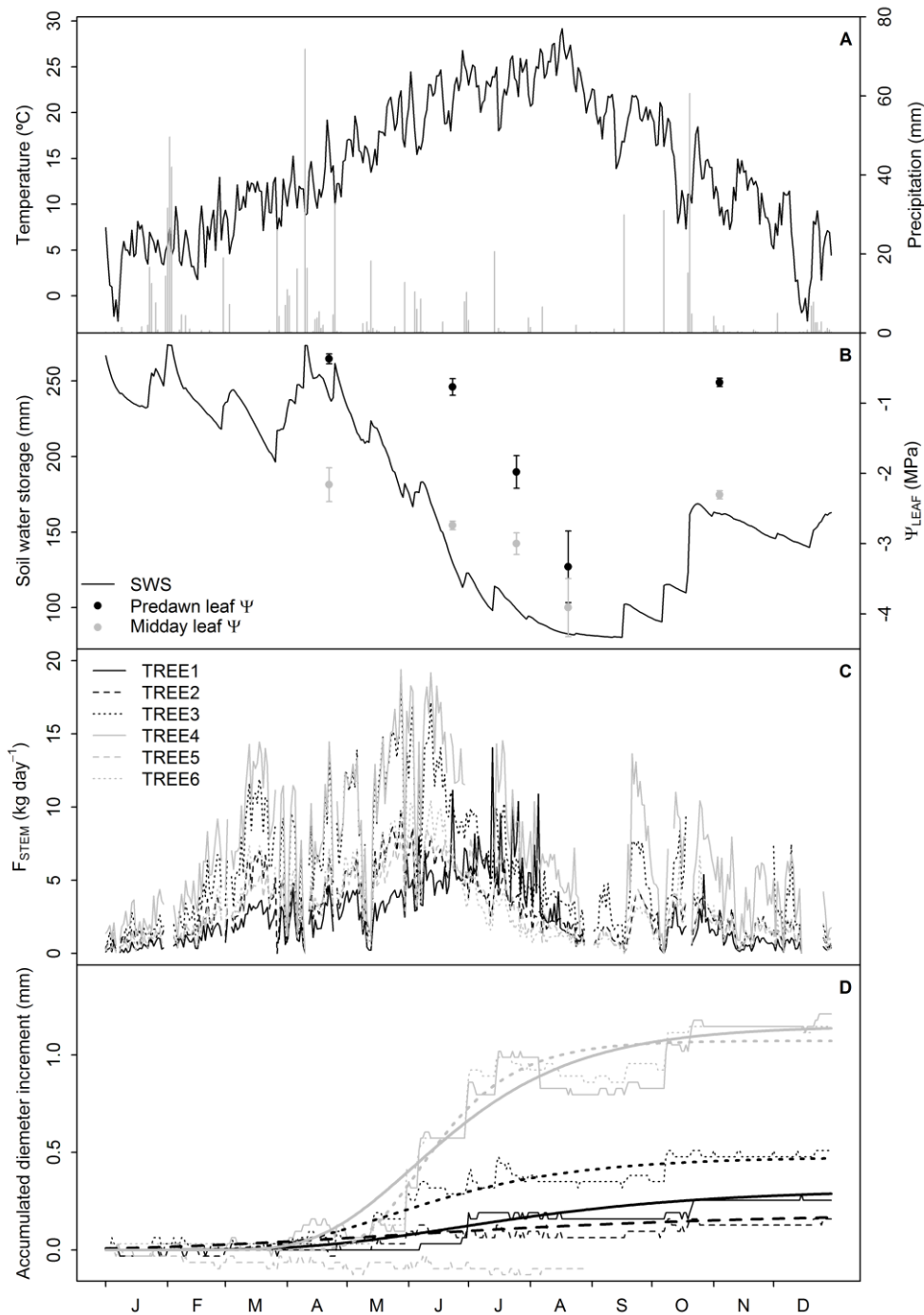


658

659 Curves of accumulated diameter increment were smoothed according to the Gompertz´s equation

660 (dashed lines). Diel variations in diameter are not shown for clarity.

661    **Figure 2.** Normalized final prediction error (FPE) of four tested models with constant or variable

662    hydraulic resistance ($R_X$) and capacitance ($C_S$) to compare model performance. Models were used to

663    simulate hydraulic functioning of *Quercus ilex* trees under wet (A) and dry (B) conditions.
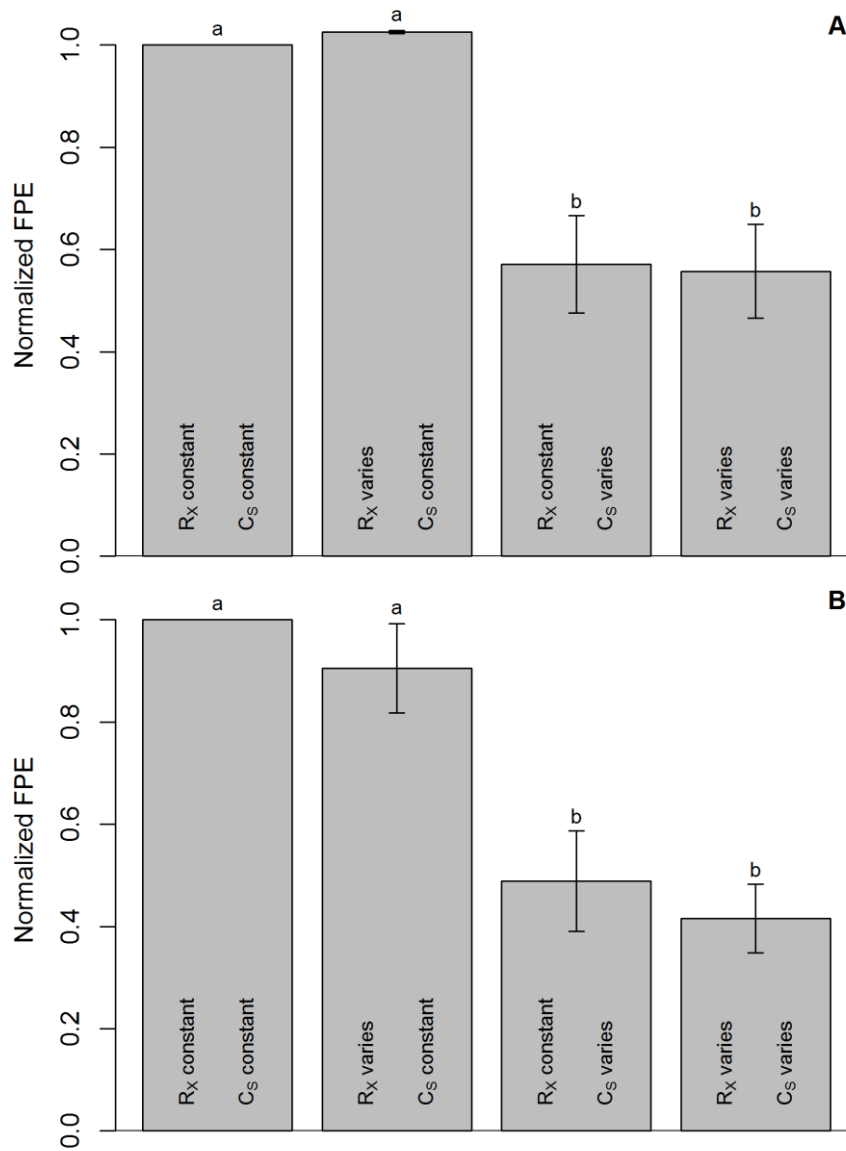


664

665    The FPE evaluates the accuracy of simulated diameter variations ($\Delta D$) and xylem water potential ($\Psi_X$)
666    and penalizes over-parameterized models. Low FPE values indicate better model performance.
667    Values of FPE were normalized relative to the model with constant $R_X$ and $C_S$ to remove inter-stem
668    variability associated to the number of observations. Normalized FPE was averaged among six trees.
669    Different letters show significant differences ($P < 0.05$).

**Figure 3.** Measured and simulated water potentials (A, D), diameter variations (B, E) and water flows (C, F) in *Quercus ilex* trees during the wet (A-C) and the dry (D-F) season. Predawn water potential ($\Psi_{PD}$) and sap flow ($F_{STEM}$) (continuous black lines) were used as model inputs, whereas diameter variations and xylem water potential ($\Psi_X$) (black dots) were used for calibration purposes.
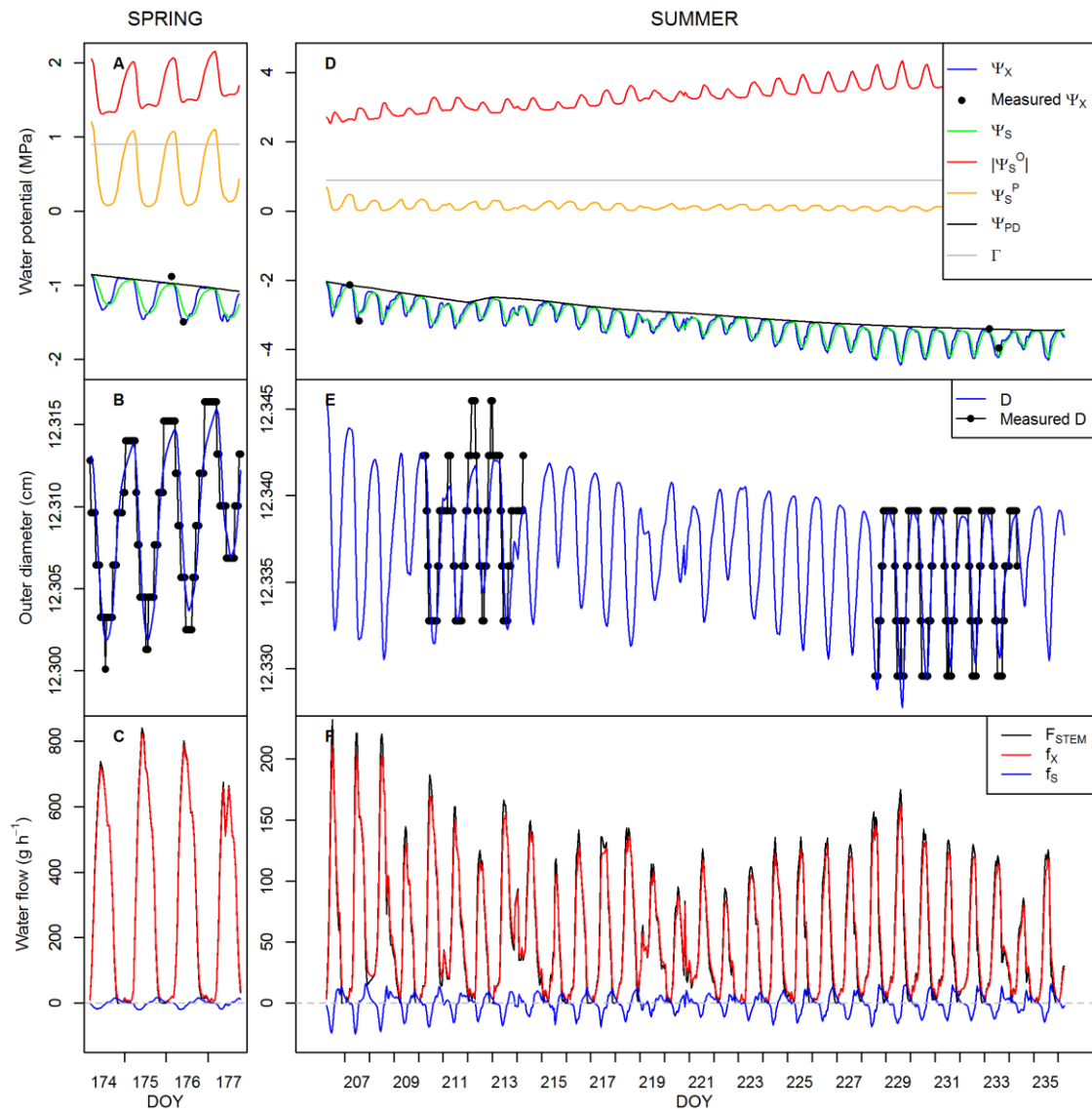


This figure displays an example of model simulation for a single tree (TREE6) when the hydraulic resistance and hydraulic capacitance were allowed to vary with predawn water potential (best model obtained). Under well-watered conditions, cell turgor ($\Psi_S^P$) at night-time exceeded the critical value for wall-yielding ($\Gamma$) (A) resulting in irreversible stem growth (B). During summer drought, $\Psi_S^P$ never exceeded $\Gamma$ (D) and irreversible stem growth was impeded (E). The storage compartment supplied water to the xylem to fulfill transpiration requirements during the morning (negative $f_S$) and was refilled during the afternoon (positive $f_S$) (C, F). Radial water exchange caused diel patterns of stem shrinkage and swelling. Note different scales for the same variables in wet and dry periods. Note that absolute values of osmotic water potential ($\Psi_S^O$) are displayed for clarity.

684    **Figure 4.** Variation in daily sap flow (A; $F_{STEM}$), daily stem water release (B; $|f_S|$), and the contribution

685    of $|f_S|$ to $F_{STEM}$ (C) in *Quercus ilex* trees along a gradient of predawn water potential ($\Psi_{PD}$).
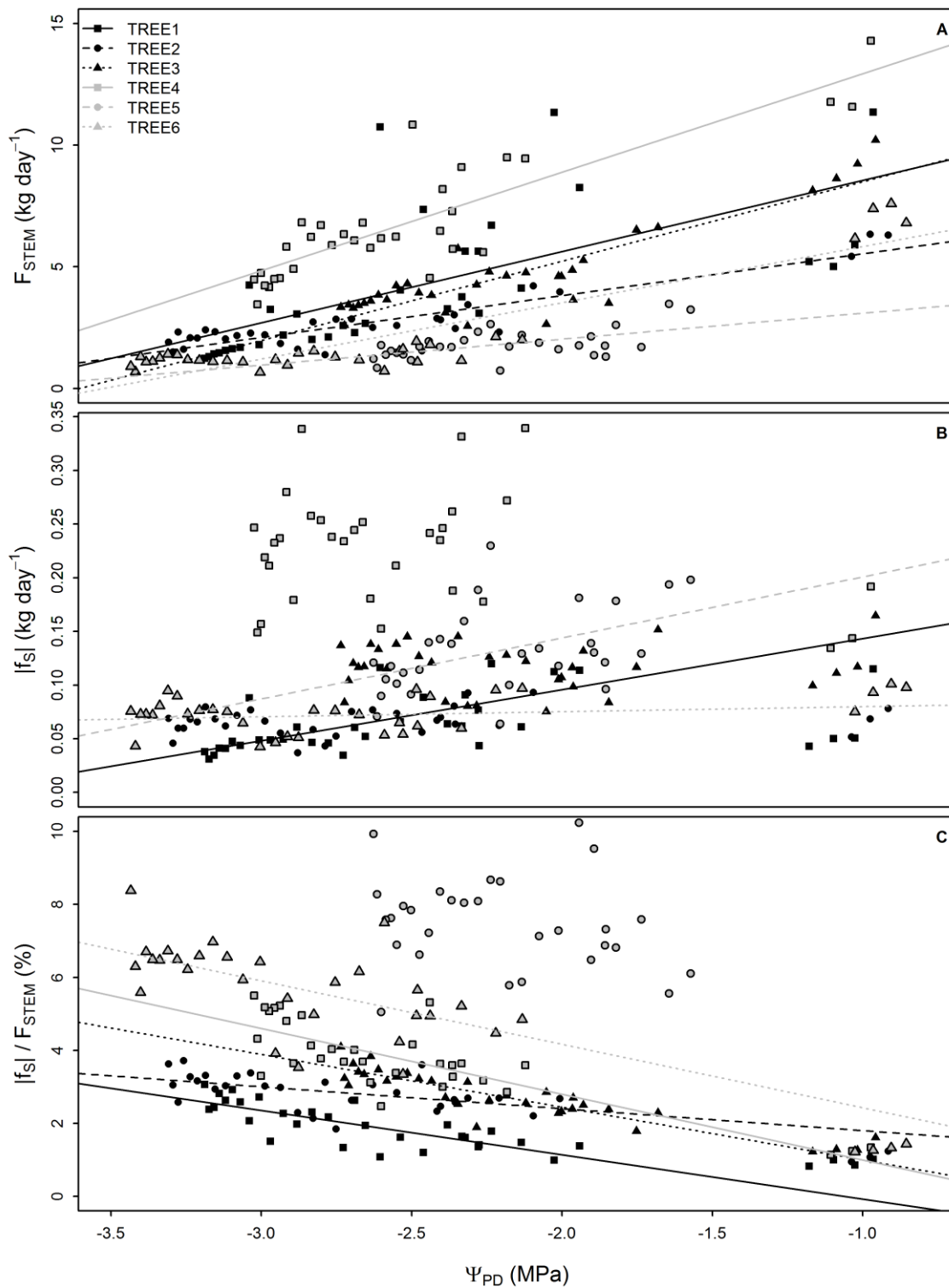


686

687    Data from model simulations in early summer (wet period) and summer drought (dry period) are
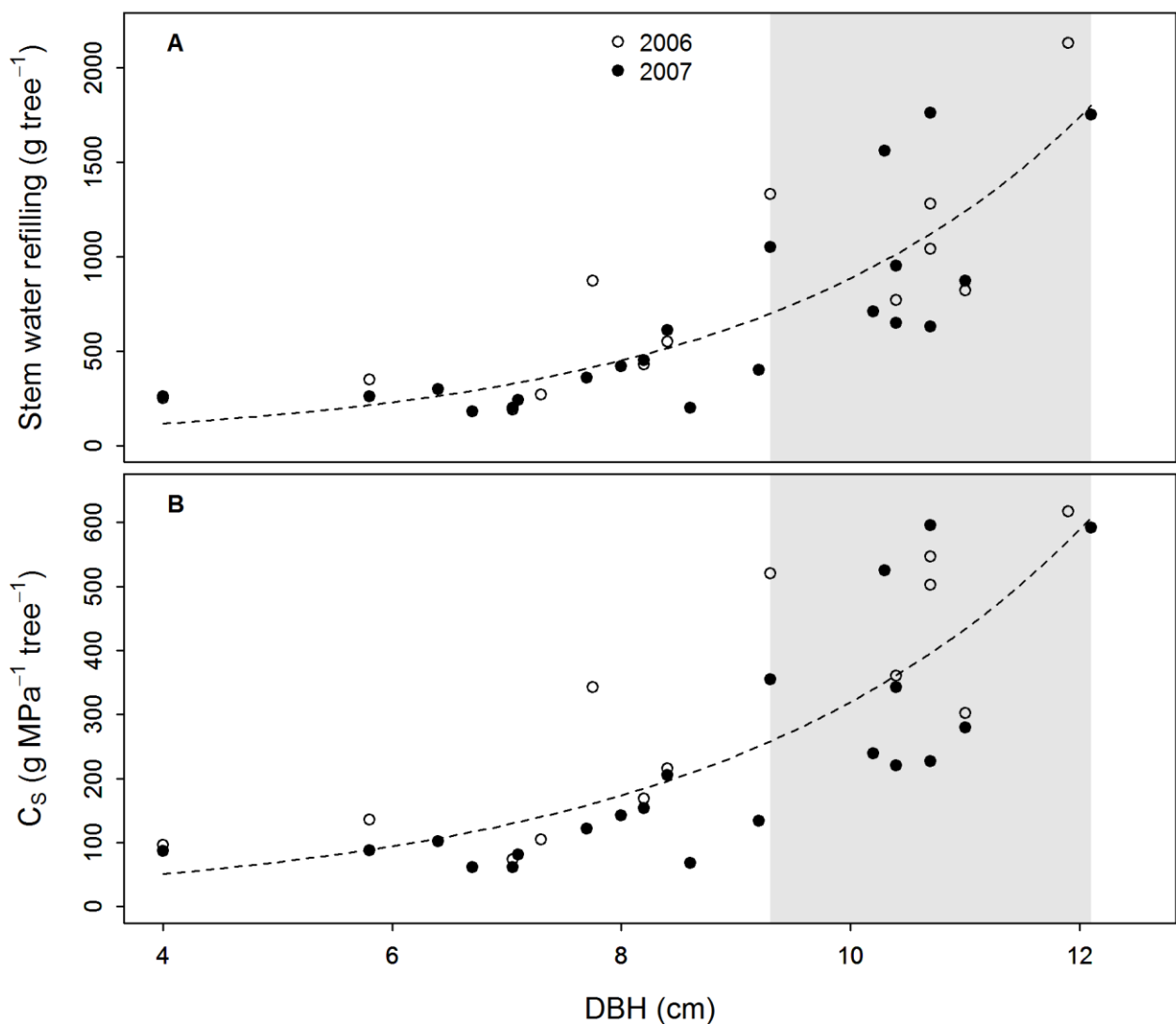688    pooled. Only significant regressions are depicted (P < 0.05).

**Figure 5.** Hydraulic capacitance ($C_S$) and cumulative water released at the tree level (A), and hydraulic

resistance ($R_X$) and conductance ($K_X$) in the root–to–leaf continuum (B) along a gradient of predawn

water potential ($\Psi_{PD}$).



692
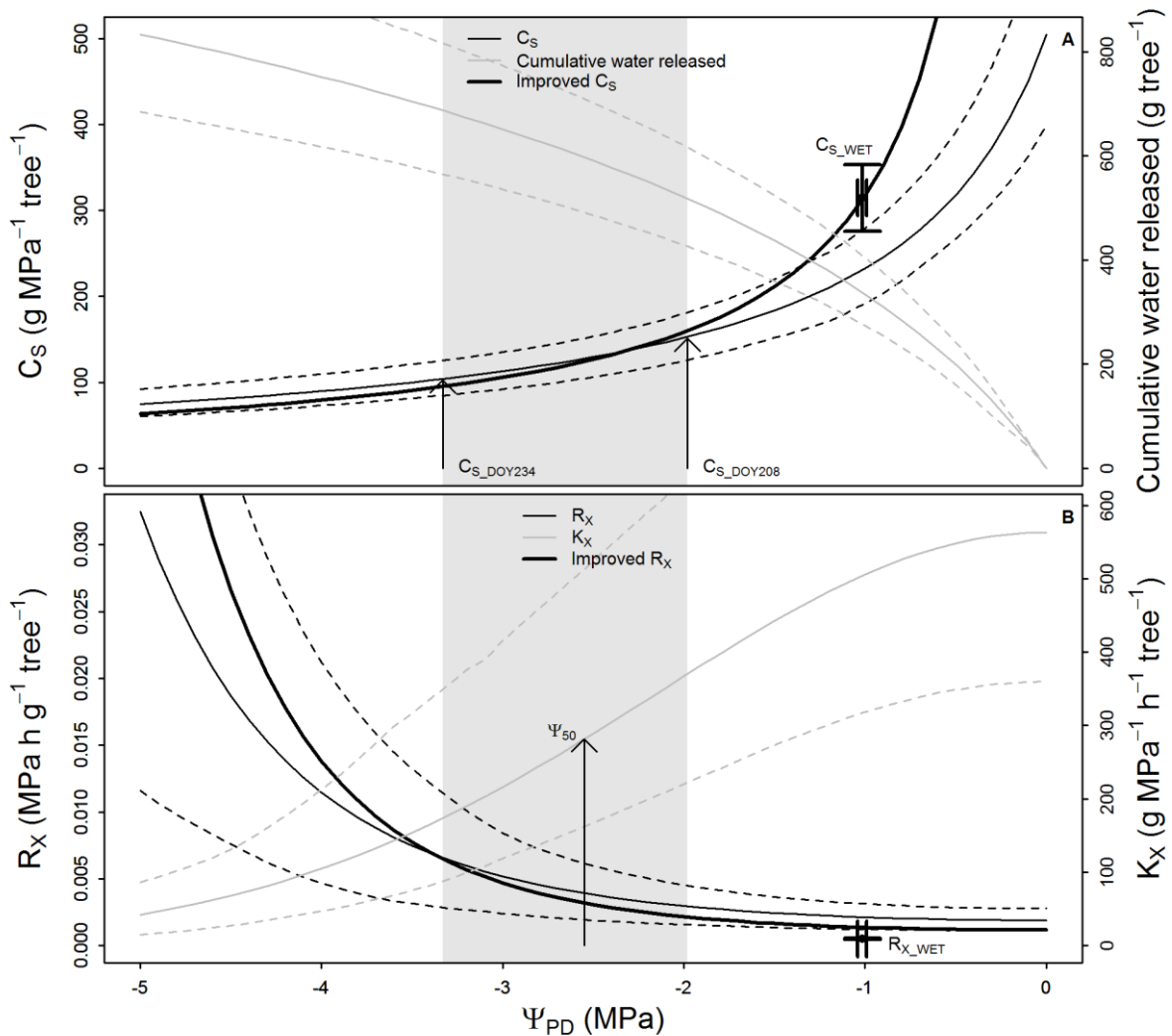
Calibrated parameters obtained from six *Quercus ilex* trees during the dry period (Table 3) were used
to estimate the mean (continuous line) and 95th and 5th percentile (dashed lines) curves of each
variable. The calibrated parameters were obtained from a mechanistic model in which $R_X$ (Eqn. 1)
and $C_S$ (Eqn. 4) were allowed to vary with $\Psi_{PD}$. Shaded areas indicate the modelled dry period, when
average $\Psi_{PD}$ ranged between -1.98 and -3.33 MPa. The curves of $C_S$ and $R_X$ adjusted for long-term
(one-month) simulations of the dry period (in black) were improved by including values of the short-
term (3-4 days) calibrations of the wet period (in red).

**Figure 6.** Stem water refilling (A) and hydraulic capacitance ($C_S$) (B) at the tree level estimated after

the first heavy rain following the dry season. Two rain events registered in 2006 and 2007 (open and

closed circles, respectively) met the minimum requirements to estimate stem storage capacity. Stem

water refilling and $C_S$ were estimated for a total of 23 *Quercus ilex* trees ranging in diameter at breast

height (DBH) from 4 to 12.1 cm. Stem water refilling and $C_S$ were exponentially related to tree DBH

(Stem water refilling = $30.27 \times e^{(0.34 \times DBH)}$; $C_S = 15.05 \times e^{(0.31 \times DBH)}$; $P < 0.001$). Shaded areas indicate the

range in DBH of trees additionally surveyed for modelling.